Dendrimer−Dendrimer Copolymer Melts

Gloria E. Rios and Galen T. Pickett*

Department of Physics and Astronomy, California State University Long Beach, 1250 Bellflower Boulevard, Long Beach, California 90840

Received August 12, 2002

ABSTRACT: We determine the strongly segregated phase boundaries between block copolymers formed by joining dendrimers of different generations by their central segments. In all cases, the phase lines between the classical diblock phases are skewed toward keeping the more highly branched species on the exterior of the curved microsegregated domains. Calculations in both the Alexander−de Gennes and classical path self-consistent field model agree well for the predicted phase boundaries.

1. Introduction

Dendritic molecules have received much attention since their invention,[1] partly because of their intriguing architecture, but more importantly for their promise in producing materials of decidedly interesting properties.[2,3] Single dendrimers can be synthesized with very extremely regular architecture, and are capable of forming thermally tunable complexes as drug-delivery agents.[4] Their well-characterized size and relative stiffness makes them suited to forming complex two-dimensionally packed arrays that can then be decorated or etched to produce nanoscopically patterned surfaces.[5] Also, the geometric proliferation of chain tips, each capable of being tagged with a biospecific functionality, makes them an ideal material for engineering smart surfaces.[6] It should be pointed out that most naturally occurring biologically relevant molecules are either lightly branched (the three-armed fatty acids) or linear (phospholipids, DNA, and proteins), and it is therefore entirely possible that hyperbranching in and of itself can grant unusual single-molecules properties with no natural analogue.

Related to these dendrimers are dendritic polymers, where the branching points are connected by flexible spacer polymers of a controllable molecular weight and composition. In some respects, these dendritic polymers resemble polymer stars,[7] with a general splaying of their many free arms away from a dense core. Indeed, miktoarm stars with an unequal number of A and B arms have been predicted to drastically reshape the AB diblock copolymer phase diagram,[8] and hyperbranched dendritic polymers are predicted to have the same effect.[9,10] The microphases are consistently skewed toward having the component with the most branches on the exterior of a curved surface, with the most pronounced effects occurring for stars with, for example, a single A type arm and many B arms. Similarly, when the A block is a linear flexible homopolymer, and the B block is a *G*-generation dendritic polymer, the phase diagram is skewed considerably toward keeping the branched block on the exterior of the cylindrical and spherical domains. For example, it was found that for compositionally symmetric "tadpole" copolymers,[11] the lamellar phase is stable when the branched block is G1−5, while the cylindrical phase obtains for G6−8, and the spherical phase occurs for G9 and more branches.[10]

The purpose of the present work is to extend earlier treatments of this system which had been limited to this most dramatic case to the situation in which the A and B blocks of the copolymer are both dendrimers of independent generation. Thus, we investigate the strong-segregation limit for GA−GB block copolymers, and determine the phase boundaries between the "classical" block copolymer phases. In the lamellar phase (L), each of the branched blocks stretches away from the flat AB interface, producing a layered material as in Figure 1. There are two cylindrical phases, one (CA) with the A material forming a cylindrical core with the B phase forming a continuous matrix in which the A cores are hexagonally packed. The second cylindrical phase (CB) has the B material confined to the cores, while the A material forms the continuous matrix. Likewise there are two spherical phases, SA and SB, in which one material is confined to spherical domains packed on a bcc lattice, while the other material forms a continuous matrix. Denoting ϕ_A and ϕ_B the overall compositions of the single dendriblock copolymers, the phase boundaries will be controlled by the overall composition and the generations of the A and B blocks, $\phi_B(G_A, G_B)$. The transitions between these phases will always follow the sequence SA−CA−L−CB−SB as ϕ_B is increased. The calculations we make are in the spherical/cylindrical unit cell approximation, and rule out a priori exotic bicontinuous phases.

The first set of calculations we employ involve the Alexander−de Gennes approximation.[9,12,13] We assume that all of the A tips and the B tips reside on the same surfaces. In the L phase, this results in the A tips being segregated to a single surface extending away from the AB interface, and similarly for the B tips. In the C phases, the outer block tips all reside on a cylindrical surface enclosing the core cylinder, while the inner tips are brought toward the center axis of the core, and similarly for the S phases. It should be noted that the L phase thus resembles back-to-back brushes of dendritic molecules, while the C phase resembles the conformation of single dendrimer−comb copolymers, where dendrimers are grafted to a single flexible backbone chain at regular lengths.[2] The S phase resembles the single-molecule conformation of an individual dendrimer molecule. Thus, the Alexander approximation can be seen as being similar to the de Gennes and Hervet ansatz for a "hollow-core" dendrimer.[14] The "filled-core" picture of Muthukumar and Lescansec,[15] however, seems to be theoretically and experimentally a more sound description. Indeed, al-

* Corresponding author.

10.1021/ma021306o CCC: $25.00
Published on Web 03/26/2003

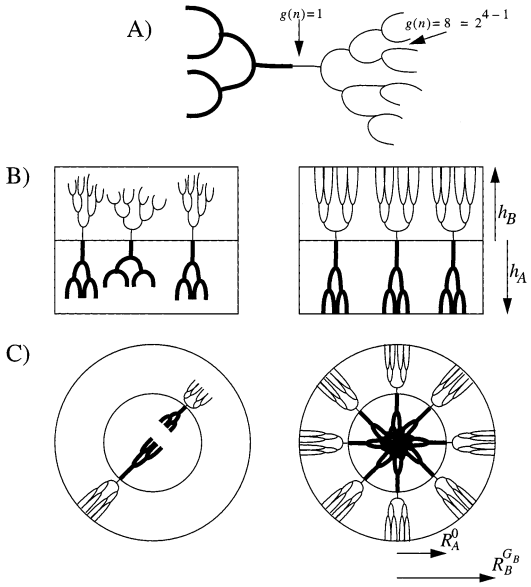

Figure 1. Schematics. (A) Schematic of a GA3GB4 dendrimer−dendrimer copolymer. The A block has 3 generations, and a total of $2^3 - 1 = 7$ dendritic arms and $2^{3-1} = 4$ free tips. The function $g(n)$ gives the number of statistically equivalent dendritic arms for a chemical index n. The chemical index counts how many monomers there are between a test monomer and the AB junction going along a direct path. (B) The left panel shows some typical chain conformations in the lamellar phase in the classical path calculation, while the right panel shows the chain conformations assumed in the Alexander−de Gennes model. The classical path scenario allows the chain tips to arrange themselves in equilibrium, while the Alexander scenario localizes the free ends on common surfaces. (C) The cylindrical and spherical phases as in part B. The radius of the AB interface is denoted $R_A{}^0$ while the overall radius of the domain is $R_B{}^{G_B}$, quantities defined in section 2.

lowing the tips of the internal and external dendrimer to occupy the entire lamellar/cylindrical/spherical domain turns out to be a more realistic assumption. In the strong-segregation limit, relaxing the confinement of the chain free ends is achieved in the so-called "classical limit"[16,17] of the Edwards self-consistent field.

The paper is organized as follows. We initially describe the Alexander−de Gennes calculation and then the classical path approximation. Then, the phase diagrams for the dendrimer−dendrimer copolymer will be developed. The results herein rest on the stong-segregation limit, the robustness of which can be determined in a simple random phase approximation (RPA) calculation. Finally, our conclusions will be offered.

2. Alexander−de Gennes Model

In the Alexander model, we assume that each copolymer has all of its branched free ends (2^{G_B-1} such ends for the B block, and similarly for the A block) confined to the same flat surfaces (lamellar phase) or cylindrical and spherical surfaces. As in Figure 1, the internal branchings of the chains are likewise held on concentric surfaces of the same geometry. As a result of space filling, the width of these domains is largest at the core (edge for the lamellar phase), decreases toward the AB interface, and then increases again toward the edge of the domain. While the details of this model have been worked out for the GA1GB case, (with the GA1 chains located on the interior of the copolymer domains) we will briefly recap that development here.[9] Additionally, we use the notation GAxGBy to denote the copolymer with x generations in its A block, and y in its B block. When the blocks have the same branching, we use the notation GxGx.

The system is made up of diblock copolymers consisting of branched A blocks, with a total degree of polymerization N_A and branched B blocks of total degree of polymerization N_B. The A block contains G_A generations, and the B block contains G_B generations, with two branches per branch point in each block. The total molecular weight of each copolymer is $N = N_A + N_B$, and ϕ_B is given by

$$\phi_B = \frac{N_B}{N} \tag{1}$$

The B block is broken up into $2^{G_B} - 1$ linear blocks, each of molecular weight n_B:

$$n_B = \frac{\phi_B N}{2^{G_B} - 1} \tag{2}$$

A similar expression holds for n_A, with $\phi_A = 1 - \phi_B$.

In the lamellar phase, the width of the lamellar pattern, h, is allowed to come to equilibrium, where $h = h_A + h_B$ with h_A being the width of the A layer and similarly for B. Making σ stand for the number of chains per unit area at the AB interface, and using $a^3 \equiv 1$ as the volume for both A and B monomers, one can generate the following relationships:

$$h_A = \sigma(1 - \phi_B)N \tag{3}$$

$$h_B = \sigma\phi_B N \tag{4}$$

The energy for the lamellar phase is calculated by obtaining the stretching energy for each block. In the Alexander−de Gennes picture, all 2^{G_A-1} ends of the A block are held at the same distance, h_A above the AB interface located at $z = 0$, while the 2^{G_B-1} ends of the B block are located at $z = -h_B$. The layer then resembles G_A brushes of A chains, each more strongly stretched as they move away from the AB interface, and similarly for the B layers. It is a simple matter, as in ref 9 to show that

$$F_{\text{stretch}} = \frac{h^2}{2N}[(1 - \phi_B)\sum_{i=0}^{G_A-1} 2^{3i} + \phi_B \sum_{i=0}^{G_B-1} 2^{3i}] \tag{5}$$

or

$$F_{\text{stretch}} = \frac{h^2}{14N}[(1 - \phi_B)(8^{G_A} - 1) + \phi_B(8^{G_B} - 1)] \tag{6}$$

With γ as the interfacial energy between A and B monomers, the total free energy per dendrimer in the lamellar phase can be written as

$$F_{\text{lamellar}}[h] = \frac{\gamma N}{h} + \frac{h^2}{14N}[(1 - \phi_B)(8^{G_A} - 1) + \phi_B(8^{G_B} - 1)] \tag{7}$$

Allowing h to adopt its equilibrium value is accomplished by choosing h^* so that $F_{\text{lamellar}}[h^*]$ is a minimum:

$$h^* = 7^{1/3}\gamma^{1/3}N^{2/3}[(1 - \phi_B)(8^{G_A} - 1) + \phi_B(8^{G_B} - 1)]^{-1/3} \tag{8}$$

so that the equilibrium lamellar free energy per chain is given by

$$F^*_{\text{lamellar}} = \left|\frac{27}{56}\right|^{1/3}\gamma^{2/3}[(1-\phi_B)(8^{G_A}-1) + \phi_B(8^{G_B}-1)]^{1/3} \quad (9)$$

It only remains to determine the free energies in the other morphologies in order to determine the location of the thermodynamic transitions between the classical diblock morphologies.

In the cylindrical phase, the chains are not stretched out uniformly, but rather their rate of stretching is determined through the constraint that the chain fills space (incompressibility). As in the lamellar phase, the cylindrical domains break up into layers which are successively thicker as they move away from the AB interface. For definiteness, let us begin with the A-core cylindrical domains (the B-core domains can be easily dealt with, and indeed the spherical domains). Again, σ stands for the total number of chains per unit area at the AB interface. The core of the micelle can be broken up into cylindrical shells of radii $R_A{}^0 > R_A{}^1 > R_A{}^2 > \ldots > R_A{}^{G_A} = 0$. Here, $R_A{}^0$ is the radius of the AB interface, and $R_A{}^{G_A} = 0$ marks the center axis of the cylinder. These radii are related through the requirement that the chains in each concentric domain fill space:

$$\pi(R_A{}^{G_A-1})^2 = n_A 2^{G_A-1}\sigma(R_A{}^0)2\pi \quad (10)$$

In short, the innermost cylindrical core has its volume spanned by chain segments composed of n_A monomers. The total number of copolymers per unit length along the cylinder is $\sigma 2\pi R_A{}^0$, and for each copolymer, there are 2^{G_A-1} of the most-branched substrands. Moving from the innermost core outward, the relationship for the ith domain reads:

$$\pi(R_A{}^i)^2 - \pi(R_A{}^{i+1})^2 = n_A 2^i \sigma R_A{}^0 2\pi \quad (11)$$

Equations 10 and 11 comprise a set of equations which can be solved numerically for the $R_A{}^i$. Similarly, the radii of the concentric B domains can be found:

$$\pi(R_B{}^1)^2 - \pi(R_B{}^0)^2 = n_B \sigma R_A{}^0 2\pi \quad (12)$$

where $R_B^0 = R_A^0$ is the radius of the AB interface, and $R_B{}^{G_B}$ is the total size of the cylindrical domain. The rest of the B layers are controlled through

$$\pi(R_B{}^i)^2 - \pi(R_B{}^{i-1})^2 = n_B 2^{i-1}\sigma R_A{}^0 2\pi \quad (13)$$

Additionally, we must have $R_A{}^0$ and $R_B{}^{G_B}$ related through

$$\phi_B = 1 - \left|\frac{R_A{}^0}{R_B{}^{G_B}}\right|^2 \quad (14)$$

With this, there is a single length scale to be determined, namely the overall size of the cylinder, $R_B{}^{G_B}$, which can be related to the total number of chains in the micelle, and σ, the number of chains per unit area at the AB interface. The total number of chains is $2\pi R_A{}^0\sigma$, so that

$$2\pi R_A{}^0\sigma N = \pi(R_B{}^{G_B})^2 \quad (15)$$

Thus, the free parameter that will be allowed to vary so as to establish equilibrium can be taken as $R_B{}^{G_B}$, the overall size of the cylinder.

Knowing the distances that each of the chain segments are stretched allows the computation of the stretching energy for the entire copolymer. A single chain segment traversing $R_A{}^1$ to the AB interface at $R_A{}^0$ entails a stretching free energy cost:

$$F^{\text{one-chain}}_{\text{stretching}} = \int_0^{n_A} dn \frac{1}{2}\left|\frac{dr}{dn}\right|^2 = \int_{R_A{}^1}^{R_A{}^0} dr \frac{1\,dr}{2\,dn} \quad (16)$$

where again, we take the monomer size $a = 1$. In order for this single chain segment to occupy all of its alloted lateral area at each r, the chain stretching must be of the form

$$\pi r dr = \sigma R_A{}^0\, 2\pi\, dn \rightarrow \frac{dr}{dn} = \frac{2R_A{}^0\sigma}{r} \quad (17)$$

so that

$$F^{A0}_{\text{stretching}} = R_A{}^0\sigma \log[R_A{}^0/R_A{}^1] \quad (18)$$

denoting the stretching energy for a single arm in the "0"th layer of the A domain. The stretching energies for the subsequent layers are thus

$$F^{Ai}_{\text{stretching}} = \frac{(R_B{}^{G_B})^2}{2N}\log\frac{r_A{}^i}{r_A{}^{i-1}} \quad (19)$$

where we have introduced the scaled radii, $r_A{}^i = R_A{}^i/R_B{}^{G_B}$. A similar expression for the B layers exists, with $r_A{}^i \rightarrow r_B{}^i$ throughout. Then, the full stretching energy per chain can be written as

$$F_{\text{stretching}}[\phi_B] = \frac{(R_B{}^{G_B})^2}{2N}\Big[\sum_{i=0}^{i=G_A-1} 2^i F^{Ai}_{\text{stretching}} + \sum_{i=0}^{i=G_B-1} 2^i F^{Bi}_{\text{stretching}}\Big] \quad (20)$$

Note that the dependence on the volume fraction of B monomers, ϕ_B is determined entirely through the space-filling relations determining the r_A's and r_B's.

As eq 19 indicates, however, the innermost domain has to be handled differently, as the Alexander contribution to the stretching energy of a chain emanating from the center of the cylinder out to $R_A{}^{G_A}$ is infinite. In this case, we take (as in ref 9) the end-distributed calculation for the free energy per chain in a convexly curved brush:

$$F^{AG_A-1}_{\text{stretching}}[\phi_B, R_B{}^{G_B}] = \frac{\pi^2}{8}\frac{[R_A{}^{G_A-1}]^2}{n_A} = \frac{(R_B{}^{G_B})^2}{N}\left[\frac{\pi^2}{8}(r_A{}^{G_A-1})^2\frac{N}{n_A}\right] \quad (21)$$

Then, as in the lamellar phase, the equilibrium $R_B{}^{G_B}$ is determined through the minimization of

$$F_{\text{cylinder}}[R_B^{G_B}] = \frac{\gamma}{\sigma} + F_{\text{stretching}}[\phi_B, R_B^{G_B}] = \frac{\gamma N}{R_B^{G_B}}(1-\phi_B)^{1/2} + F_{\text{stretching}}[\phi_B, R_B^{G_B}] \quad (22)$$

The minimization of $F_{\text{cylinder}}[\phi_B, R_B^{G_B}]$ with respect to $R_B^{G_B}$ is straightforward.

The calculation for the spherical geometry is very similar to the cylindrical calculations. The radial shells are determined by space filling as in the cylindrical case:

$$\frac{4\pi}{3}[(R_A^{\,i})^3 - (R_A^{\,i+1})^3] = n_A 2^{i-1}\sigma[R_A^{\,0}]^2 4\pi \quad (23)$$

while ϕ_B and σ are related to the size of the cylindrical domains through

$$\phi_B = 1 - \left|\frac{R_A^{\,0}}{R_B^{G_B}}\right|^3 \quad (24)$$

and

$$4\pi[R_A^{\,0}]^2\sigma N = \frac{4\pi}{3}[R_B^{G_B}]^3 \quad (25)$$

Nonuniform stretching of the chains in this case requires that

$$4\pi r^2 \mathrm{d}r = \sigma R_A^{\,i}\, 2^i 4\pi\, \mathrm{d}n \rightarrow \frac{\mathrm{d}r}{\mathrm{d}n} = \frac{R_A^{\,i}\sigma}{r^2} \quad (26)$$

so that

$$F_{\text{stretching}}^{Ai} = [R_A^{\,0}]^2 2^{i-1}\sigma\left[\frac{1}{R_A^{\,i}} - \frac{1}{R_A^{\,i+1}}\right] \quad (27)$$

Thus, the free energy per chain can easily be calculated numerically, in both the lamellar, cylindrical and spherical phases. It should be kept in mind, however, that there are two distinct cylindrical as well as spherical phases. These can be determined by labeling the material inside the core, e.g., the SA phase stands for the spherical phase with the A chains on the interior of the core, and SB likewise. Thus, given G_A, G_B, the volume fractions denoting changes of morphological stability can be labeled S−C/A, C−L/A, C−L/B, S−C/B, as ϕ_B increases.

3. Classical Path Model

Again, the polymers in question have an A block consisting of a regularly branched dendritic polymer of G_A generations with monodisperse flexible spacers of molecular weight n_A, joined to a B block consisting of a regularly branched dendritic polymer of G_B generations, with monodisperse flexible spacers of molecular weight n_B, as in Figure 1. Thus, the GA1−GB1 species is an ordinary diblock copolymer, with total molecular weight $n_A + n_B$, and the volume fraction of B monomers, ϕ_B satisfying eqs 1 and 2. In the strong segregation limit, the phase boundaries between the lamellar, cylindrical, and spherical "classical" phases should be entirely a function of ϕ_B as well as G_A and G_B. As in ref 9, we expect these phase boundaries to be shifted significantly toward keeping the branched block on the *exterior* of the curved microdomains. To determine these phase boundaries, we need to compare $F_{\text{lam}}(\phi_B, G_A, G_B)$ to $F_{\text{cyl}}(\phi_B, G_A, G_B)$ to $F_{\text{sph}}(\phi_B, G_A, G_B)$. In each case, the morphology with the lowest free energy per chain is the equilibrium phase.

Let us begin with the calculation for $F_{\text{lam}}(\phi_B, G_A, G_B)$. While the overall fraction of B monomers is fixed by the chemistry of the chain, eq 1, the overall *width* of the lamellar pattern is not. As above, $h = h_A + h_B$ is the total width of a single lamellar half-layer (so that the bulk pattern has a total repeat spacing of $2h$). Let σ be the number of chains per unit area at the A − B interface. The fact that we consider meltlike conditions requires

$$\phi_B = h_B/h \quad (28)$$

$$N = h/\sigma \quad (29)$$

so that h_A and h_B can be written in terms of σ and ϕ_B

$$h_A = (1-\phi_B)N\sigma \quad (30)$$

$$h_B = \phi_B N\sigma \quad (31)$$

where we again set the volume a single monomer takes up in the melt $a^3 = 1$.

To calculate $F_{\text{lam}}(\phi_B, G)$, we can independently calculate the free energy per A block, F_A, the free energy per B block, F_B, and the interfacial energy per chain, F_{surf}. Here, each block forms a dendrimer−brush. We let

$$F_A = \frac{h_A^{\,2}}{N_A} f(G_A) \quad (32)$$

where $f(G_A)$ is the average dimensionless free energy per dendrimer in a GA-generation dendrimer brush. While this scaling will be verified below (and occurs naturally in eq 6 and eq 20 in the Alexander model), it is necessary as a result of the Gaussian origin of the conformational part of the single-chain free energy. The typical distance the A blocks are stretched is h_A, and a linear chain of $G_A n_A$ monomers connects each free tip with the central monomer at the AB interface. The scale of the Gaussian entropy is then

$$F_A \sim h_A^{\,2}/(G_A n_A) f'(G_A) = h_A^{\,2}/N_A[G_A^{\,-1}(2^{G_A} - 1)f'(G_A)] \quad (33)$$

The term in brackets in eq 33 depends only on G_A, and we have combined them into the single unknown function, $f(G_A)$.

Now, if the surface energy between A and B monomers is γ, then the surface energy per chain is simply

$$F_{\text{surf}} = \frac{\gamma}{\sigma} \quad (34)$$

Thus, the free energy per chain is

$$F_{\text{lam}}[\sigma] = F_A + F_B + \frac{\gamma}{\sigma} = N\sigma^2((1-\phi_B)f(G_A) + \phi_B f(G_B)) + \frac{\gamma}{\sigma} \quad (35)$$

Minimizing $F_{\text{lam}}[\sigma]$ with respect to σ determines equilibrium coverage at the AB interface

$$\sigma_{\text{eq}} = 2^{-1/3}\gamma^{1/3}N^{-1/3}[(1-\phi_B)f(G_A) + \phi_B f(G_B)]^{-1/3} \quad (36)$$

so that

$$F_{\text{lam}} \equiv F_{\text{lam}}[\sigma_{\text{eq}}] = (3)(2^{-2/3})\gamma^{2/3}N^{1/3}[(1-\phi_{\text{B}})f(G_{\text{A}}) + \phi_{\text{B}}f(G_{\text{B}})]^{1/3} \quad (37)$$

Notice the familiar scaling of the lamellar free energy as $\gamma^{2/3}$ and as $N^{1/3}$ which is simply the usual strongly segregated diblock scaling.

All that remains is to determine $f(G_{\text{A}})$, the average dimensionless free energy per chain in a branched dendrimer brush. This has been calculated previously[18] in the classical path self-consistent field approximation scheme of Semenov[16] and Milner, Witten, and Cates.[17] Let us start with an appropriate free-energy functional that can be used to determine both the configuration of these branched chains and $f(G)$, by considering the A block:

$$F_{\text{chain}}[z(z_{\text{o}}, n)] = \int_0^{G_{\text{A}}n_{\text{A}}} \mathrm{d}n\, g(n)\left[\frac{1}{2a^2}\left|\frac{\mathrm{d}z}{\mathrm{d}n}\right|^2 + P(z(z_{\text{o}}, n))\right] \quad (38)$$

Here, $z(z_{\text{o}}, n)$ is the *primitive* trajectory of the dendrimer block,[18] all of whose free ends are held at $z = z_{\text{o}}$, and whose single trunk chain is attached to the $z = 0$ plane where the A and B domains meet. The function $g(n)$ counts the number of statistically equivalent chain segments as a function of chemical index. Near the free ends ($0 < n < n_{\text{A}}$ in eq 38), there are $2^{G_{\text{A}}-1}$ equivalent chain segments. As shown schematically in Figure 1 for a $G4$ block

$$g(n) = 2^{G_{\text{A}}-1} \quad \text{when } 0 \le n < n_{\text{A}} \quad (39)$$

$$g(n) = 2^{G_{\text{A}}-2} \quad \text{when } n_{\text{A}} \le n < 2n_{\text{A}} \quad (40)$$

$$\vdots$$

$$g(n) = 1 \quad \text{when } (G_{\text{A}}-1)n_{\text{A}} \le n \le G_{\text{A}}n_{\text{A}} \quad (41)$$

The fact that each statistically identical chain segment follows exactly the *same trajectory* is true only in the classical limit, that is when Gaussian fluctuations of the chain trajectories around those minimizing $F_{\text{chain}}[z(z_{\text{o}}, n)]$ are negligible.[18]

The free energy functional in eq 38 essentially states that each of the $g(n)$ equivalent strands have to be stretched a certain amount $\mathrm{d}z$, and each of them needs to be inserted into the layer at the height $z(z_{\text{o}}, n)$ at the cost of $P(z)$ per monomer. When the A block is an unbranched G1, then it is well-known that the potential $P(z)$ is uniquely determined by the monodispersity of the chains. In the language of classical mechanics, a particle dropped the height z_{o} from rest hits the "ground" in a "time" N_{A} regardless of the initial position of the particle, z_{o}. The required potential has a parabolic form:[16,17]

$$P(z) = P_{\text{o}}(h^2 - z^2) \quad (42)$$

The required equal-time potential is *harmonic*. Since the total transit time of the classical particle is known to be one-fourth of the full oscillation period of this equivalent oscillator, we must have that[17]

$$P_{\text{o}} \equiv \frac{{\omega_{\text{o}}}^2}{2{n_{\text{A}}}^2} \rightarrow \omega_{\text{o}} = \frac{\pi}{2} \quad (43)$$

where we have introduced the dimensionless frequency of the effective oscillator, ω_{o}. When the chain is regularly branched, with statistically identical segments, we retain the form for the insertion potential per monomer as in eq 42 as an ansatz, but with a different expression for P_{o} and ω_{G}.[18] The justification for this ansatz is necessarily a posteriori, in that we will check that choosing ω_{G} correctly satisfies the monodispersity property of the chains. This monodispersity property can be cast as a nonlinear integral equation for $P(z)$,[17,20] with the existence of a unique solution guaranteed. Thus, without going into the technical details of how such an integral equation can be solved, we merely show here that the required $P(z)$ is of the form shown in eq 42.

Using this parabolic ansatz, minimizing eq 38 with respect to variations in $z(z_{\text{o}}, n)$ yields the Euler−Lagrange equation of motion:

$$\frac{\mathrm{d}}{\mathrm{d}n}\left(\frac{g(n)}{2a^2}\frac{\mathrm{d}z}{\mathrm{d}n}\right) z(z_0, n) = g(n)\frac{\mathrm{d}}{\mathrm{d}z}P(z) \quad (44)$$

With the ansatz eq 42, and the definition of P_{o} given in eq 43, this becomes

$$\frac{\mathrm{d}}{\mathrm{d}n}\frac{g(n)}{2a^2}\frac{\mathrm{d}}{\mathrm{d}n} = -\,g(n)\frac{{\omega_{\text{G}}}^2}{2a^2{N_{\text{B}}}^2}\, z(z_{\text{o}}, n) \quad (45)$$

When the chemical index is not an integral multiple of N_{A}, the factor $g(n)$ is a constant, and the equation of motion during these times is

$$\frac{\mathrm{d}^2}{\mathrm{d}n^2}z(z_{\text{o}}, n) = -\frac{{\omega_{\text{G}}}^2}{{n_{\text{A}}}^2}z(z_{\text{o}}, n) \quad (46)$$

Thus, the trajectory must be a continuous piecewise harmonic function. When the chemical index is an integral multiple of n_{A}, the weighting function $g(n)$ is cut discontinuously in half. Integrating the equation of motion from just below this discontinuity to just above it yields a boundary condition pasting together the harmonic pieces of the overall trajectory:

$$2\frac{\mathrm{d}z}{\mathrm{d}n}\Big|_{g_{n_{\text{A}}^-}} = \frac{\mathrm{d}z}{\mathrm{d}n}\Big|_{g_{n_{\text{A}}^+}} \quad \text{for each } g = 1 \ldots g = G_{\text{A}} \quad (47)$$

Thus, the *velocity* along the chain doubles at the junction points to make up for the fact that half of the chains entering the junction terminate there. Each piecewise harmonic solution to eq 45 thus has the necessary two conditions required for a unique specification. In particular, the continuity of the overall chain trajectory imposes $G - 1$ constraints, and eq 47 imposes another $G - 1$ constraints. The overall solution is then fixed by requiring that

$$z(0, z_{\text{o}}) = z_{\text{o}} \quad \text{and} \quad \frac{\mathrm{d}}{\mathrm{d}n}z(n, z_{\text{o}})\Big|_{n=0} = 0 \quad (48)$$

Thus, the chain starts its trajectory at $z = z_{\text{o}}$ with vanishing tension in the chain free ends. The unknown ω_{G} can then be determined by requiring

$$z(G_{\text{A}}n_{\text{A}}, z_{\text{o}}) = 0 \quad (49)$$

that is, the final monomer on each chain is located at the AB interface located at $z = 0$. Table 1 contains the numerical values of ω_{G} thus determined for $1 \le G_{\text{A}} \le$

Table 1. Classical Path Dimensionless Frequency ω_G,[a] as Well as the Dimensionless Free Energy Per Chain, $F_{chain}/h_B^2N_B^2 = \omega_G^2/2(2^G - 1)^2$

G	ω_G	$\omega_G^2/2(2^G - 1)^2$
1	1.570 796 326	1.233 700 550
2	0.615 479 606	1.704 668 155
3	0.339 836 909	2.829 483 562
4	0.210 910 698	5.004 373 796
5	0.138 513 684	9.218 892 573
6	0.093 821 603	17.468 547 812
7	0.064 690 633	33.748 948 737
8	0.045 074 196	66.055 100 147
9	0.031 601 121	130.381 750 822
10	0.022 236 050	258.723 914 648

[a] Note that $\omega_1 = \omega_o = \pi/2$.

10, and amounts to the required consistency check that the parabolic ansatz for $P(z)$ with ω_G as in Table 1 is the one and only equal-time potential for this situation.

One convenient property of the G1 polymers, that is an ordinary polymer brush, is that $F_{chain}[z(z_o, n)]$ is independent of z_o. The equivalent statement for a classical harmonic oscillator is that each dynamic trajectory, if followed through a complete oscillation, is associated with the *same action integral*. This property is retained for the dendrimer brush,[19] so that the single-chain free energy along the classical path is simply:

$$F_{chain}^{eq} = \int_0^{G_A n_A} dn\, g(n) \frac{\omega_{G_A}^2 h_A^2}{2a^2 n_A^2} = \frac{\omega_G^2 h_A^2}{2a^2 n_A} (2^{G_A} - 1) \tag{50}$$

The consequence of eq 50 is a great simplification in determining phase boundaries, for this result does not depend on the geometry of the phase under question. Thus

$$f_{lamellar}(G) = f_{cylindrial}(G) = f_{spherical}(G) \tag{51}$$

The dimensionless free energy per chain in each phase is identical. The essential physics behind this is that the self-consistent potential is parabolic. This result can therefore fail if there are regions in the curved domains of the cylinder or sphere phases from which chain free ends are excluded.[16,20] Such end-exclusion "dead zones" alter the self-consistent monodisperse potential, resulting in a free energy per chain that depends on the location z_o of the free end. Thus, with the presence of these dead zones, the classical energy can still be calculated, but in order to determine $f(G)$, an average over the self-consistently determined end-density $\xi(z)$ must be executed:

$$F_{chain}^{eq} = \int dz_o\, \xi(z_o) f(z_o) \tag{52}$$

where the end-density is determined by the integral equation:

$$\phi(z) = \int_0^h dz_o \frac{\xi(z_o) g(n(z/z_o))}{dz/dn} \equiv 1 \tag{53}$$

When $\xi(z_o) > 0$ for all z_o, eq 50 allows an easy calculation of the equilibrium free energy per chain in the lamellar phase:

$$F_{lam}[G_A, G_B, \phi_B] = 2^{-2/3} 3(\gamma)^{2/3} N^{1/3} [(1 - \phi_B)\omega_{G_A}^2 (2^{G_A} - 1) + \phi_B \omega_{G_B}^2 (2^{G_B} - 1)]^{1/3} \tag{54}$$

Thus, all that is really needed to calculate F_{lam} is the appropriate frequency ω_G for both the A and B blocks.

Calculating F_{cyl} and F_{sph} is thus quite simple. Let us specialize first to the case where the B material is located at the center of the cylindrical and spherical domains. The volume fraction ϕ_B of B-type monomers is related to the radius of the B core, R_B and the width of the annular domain occupied by the A monomers through

$$\frac{R_B^d}{(R_B + R_A)^d} = \phi_B \tag{55}$$

where $d = 1$ is the lamellar case, $d = 2$ corresponds to the cylindrical phase, and $d = 3$ corresponds to the spherical phase. Thus

$$R_A = R_B(1 - \phi_B^{1/d}) \tag{56}$$

Then again, according to eq 1, n_A can be chosen to give the correct ϕ_B given n_B:

$$n_A = \left(\frac{1 - \phi_B}{\phi_B}\right)\left(\frac{2^{G_B - 1}}{2^{G_A - 1}}\right) n_B \tag{57}$$

The equilibrium free energy per chain then is

$$F_{Bin}[\phi_B, G_A, G_B] = 2^{-2/3} 3(a^2\gamma)^{2/3} N^{1/3} \left[f(G_B) + (1 - \phi_B^{1/d})^2 \frac{\phi_B (2^{G_A - 1})}{(1 - \phi_B)(2^{G_B} - 1)} f(G_A) \right] \tag{58}$$

where again, $d = 1, 2, 3$ corresponds to lamellar, cylindrical, and spherical phases where B monomers occupy the core of the micelles.

The morphologies with A on the interior of the domains have an equilibrium free energy corresponding to

$$F_{Ain}[G_A, G_B, \phi_B] = F_{Bin}[1 - \phi_B, G_B, G_A] \tag{59}$$

Apart from the issue of the existence of dead zones, eq 59 gives an almost analytic expression for the dendrimer−dendrimer copolymer phase boundaries as a function of G_A, G_B, and ϕ_B. As long as the density of ends is predicted to be nonzero throughout the spherical and cylindrical domains characterized by the radius of curvature implied by eq 56, these predictions are valid. In what follows, we numerically calculate the end-density distribution, and duly note when dead zones (and hence unreliable predictions of the theory) occur. The filling-in of these dead zones with a parabolic potential is essentially a consequence of the "filled-core" conformation of single dendimer molecules.[15]

4. Results

On the basis of eq 59 for the classical path model and on the basis of eq 22, we have calculated phase diagrams for the three classical diblock phases in the spherical/cylindrical unit cell approximation. Figure 2 shows the phase boundaries for the case where the A block of the diblock is a G1 dendrimer, that is, an ordinary linear flexible polymer for the classical path model. This phase diagram has been calculated before,[10] and its properties are well understood. For this system of "tadpole"

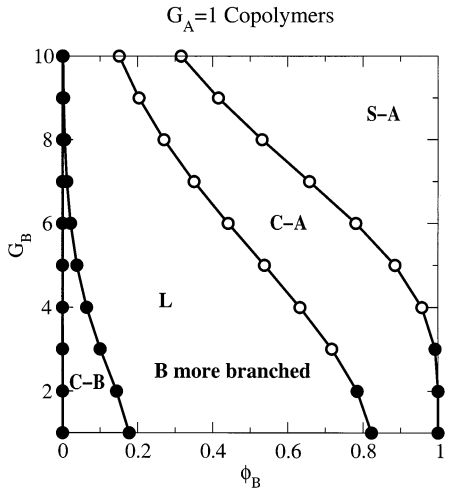

Figure 2. Phase diagrams: $G_A = 1$. End-distributed phase diagrams for $G_A = 1$ and various G_B. These "tadpole" configuration diblocks have the B branch much more highly branched than the A blocks, and as the branching generation of the B block increases, all transition lines skew toward smaller ϕ_B, thus keeping the B block on the exterior of the curved domains. The filled symbols indicate calculations with the parabolic ansatz, eq 42 which require a *negative* density of free ends, and thus represent inherently unreliable predictions. Note that the entire L−CB transition line is thus invalid. The exterior of these cylindrical domains are composed of a brush of linear A polymers grafted to the curved AB interface.

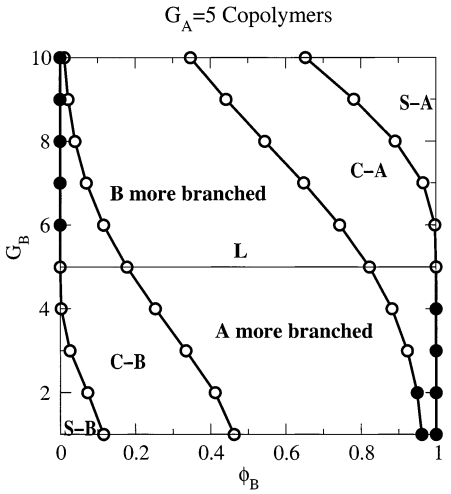

Figure 3. Phase diagrams: $G_A = 5$. The $G_B = 5$ phase diagram is indicated by the thin horizontal line. As a consequence of the fact that the dimensionless free energy per chain in the A and B blocks depends only on G_A and G_B, it must be that any copolymers with $G_A = G_B$ will have the same phase boundaries. In contrast to the $G_A = G_B = 1$ case (the x axis in Figure 2) the dead zones have been eradicated. In the region where the A block is more strongly branched, the A blocks are more readily found on the exterior of the curved domains, and the opposite occurs when the B block is most highly branched.

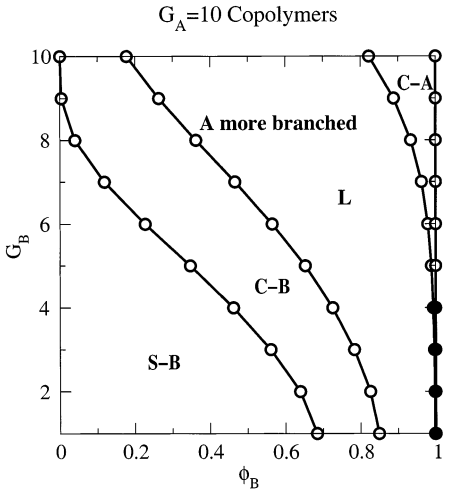

Figure 4. Phase diagrams: $G_A = 10$. Here, the A block is a G10 dendrimer, and the B block is variously branched. For the entire diagram except the top tier of points, the A block is more heavily branched than the B block. At $G_B = 10$, the A and B blocks are equivalently branched, and thus the transitions match those for the G1G1 diblock (Figure 2) and the G5G5 diblock (Figure 3). The filled in symbols indicate conditions under which a negative end density is required in order to reach melt conditions.

copolymers,[11] the B block is always more highly branched than the A block, and making the B block more branched moves all transition lines toward smaller values of ϕ_B. Note that the solid lines have no physical meaning and simply guide the eye to the corresponding transition points as the geometry of the B block is changed. For the parabolic calculation, it is clear from the diagram that the spherical phases SA and SB are pushed completely off the phase diagram for $G_A = 1$. This may be regarded as an artifact of the fact that the parabolic potential profile requires the overfilling of physical space with monomers under these conditions. Accommodating a dead zone appreciably changes the parabolic profile,[20] allowing the redistribution of chain ends toward the outer extremities of the copolymer domains. Thus, the dead zones stabilize the spherical phases against the cylindrical phases for ordinary diblocks. If we could tolerate an unphysical negative distribution of chain ends (thus relieving an overfilling of space), then there would be *no equilibrium spherical* phases at all in the diblock phase diagram. As we see blow, especially in Figures 3 and 4, those dead zones disappear for $G_A = G_B \gg 1$. The extinction of the spherical phase altogether has been noted for mikto-arm star copolymers[8] and appears here as well. For $G_A = 1$, it is clear that as G_B gets larger and larger, the spherical-A core phase SA dominates the phase diagram more and more. When $G_B = 10$, the L−CA transition occurs at only 18% volume fraction of B. Cylinders form at this point composed of a majority of A monomers crowded into a large core, surrounded by a highly stretched, but relatively thin, layer of B dendrimers. The real structure adopted under these circumstances cannot be the highly symmetric cylindrical domains used in the model calculations but must instead be highly distorted in order for the domains to properly fill space. The more complicated and numerically intensive theories of refs 21−25 are required here. At 31% volume fraction of B, spheres of A surrounded by a very thin skin of B monomers form the spherical phase. The phase diagram is biased toward keeping the more highly branched species on the exterior of the curved domains.

Note that the entire L−CB line as calculated requires negative end-density. For the entire CB phase, the A corona surrounding the B core is comprised of single homopolymers which are well-known to require a dead zone to fill space properly. This situation changes when $G_A = 5$, as in Figure 3. The G5G5 copolymer has exactly the same transitions as predicted for the diblock G1G1 case, but the necessity of dead zones to fill space has disappeared. Thus, we expect that the existence of the SB and SA phases for these copolymers to be entirely suppressed. Experimentally, the spherical phases could

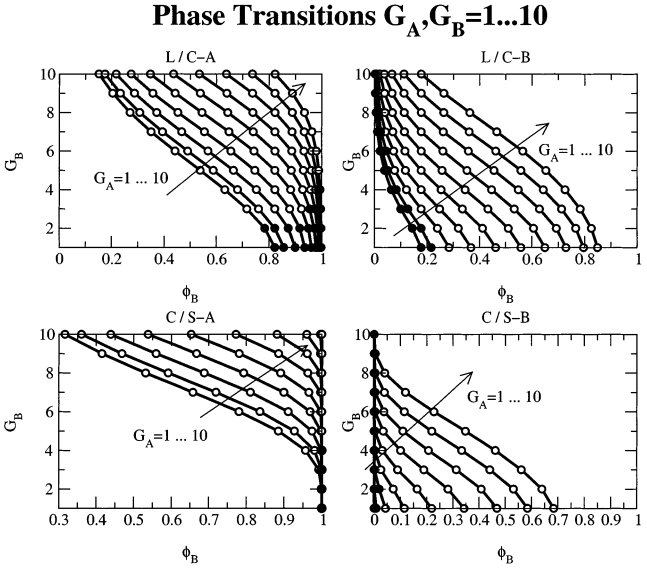

Figure 5. Phase diagrams. Here, all transitions for $G_A = 1$, ..., 10 and $G_B = 1$, ..., 10 copolymers are listed. The filled circles indicate points requiring a negative end-density for melt-conditions to be satisfied with a parabolic insertion potential. The upper-left panel shows the L−CA transitions, that is the lamellar-to-A-filled cylindrical transitions. Ten successive curves are shown for $G_A = 1$, ..., 10. The upper-right panel shows the L−CB transitions, that is, transitions from the lamellar to the B-filled cylindrical phase. The lower-left panel shows the C−SA transitions, that is the transition from A-filled cylinders to A-filled spheres, and the lower-right panel shows the transitions from B-filled cylinders to B-filled spheres, again as G_A is increased from 1 to 10 as indicated by the arrows.

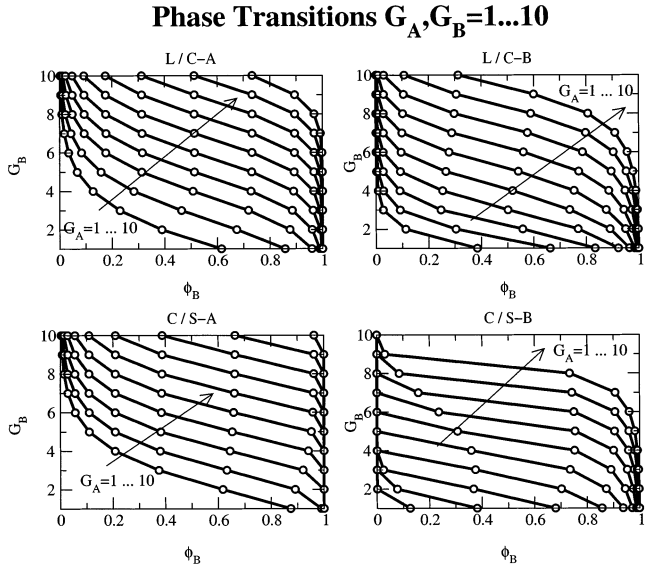

Figure 6. Alexander-de Gennes phase diagrams. As in Figure 5, transitions from SA−CA−L−CB−SB depend on the branching of both the A and B blocks. Generally, the phase boundaries are biased so as to keep the more highly branched species on the exterior of the domains.

still exist as a three-dimensionally ordered array of these spherical domains will not exhibit the spherical Wigner−Seitz cell we use here as the basis of our calculations. For $G_A \gg G_B$ or for $G_A \ll G_B$, the dead zones reappear near $\phi_B = 0$ and $\phi_B = 1$. Again, in the lower portion of the phase diagram, the A block is more heavily branched than the B blocks, so the transition points are skewed toward higher values of ϕ_B so that the A block is biased toward the outside of the domains. The situation is balanced along $G_B = 5$, where the are only three phases (two cylindrical and the lamellar phase) placed symmetrically about $\phi_B = 0.5$ as required. For the upper part of the phase diagram, the B block is more highly branched, and the phase boundaries are swept toward smaller values of ϕ_B.

Figure 4 shows the situation when the A block is a G10 dendrimer, and the B block is systematically increased in branching from G1 to G10. The essential similarity between the lower most phase boundaries (GA10GB1) and the uppermost phase boundaries in Figure 2 (GA1GB10) should be noted, and they are related though eq 59. Only as G_B becomes comparable to 10 do the phase boundaries begin to approach symmetric values, the same ones attained by the G1G1 and G5G5 dendrimers.

Figure 5 shows all transitions for 100 combinations of $G_A = 1$, ..., 10 and $G_B = 1$, ..., 10. The four panels show the transition lines for the four separate transitions that can be observed in this case. The upper-left panel shows the location of the lamellar phase to the A core cylindrical phase (L−CA), for $G_A = 1$, ..., 10. As is evident from the figure, this transition line for $G_A = 1$ and $G_A = 2$ uniformly requires negative end densities (filled circles). Increasing G_A moves all transitions toward higher values of ϕ_B, while increasing G_B moves all transitions toward lower values of ϕ_B. Thus, a great deal of control on the strongly segregated phase diagram is possible by choosing G_A and G_B. The upper right panel shows all transitions between the lamellar and the B core cylindrical phases, and the bottom two panels show transitions between cylindrical and spherical phases.

Entirely similar phase diagrams based on the Alexander−de Gennes model of ref 9 are shown in Figure 6. The physical picture differs quite a bit between the two models, but remarkably similar phase diagrams are predicted by both models. In this instance, "hollow-core" vs "filled-core" models of single dendrimers are essentially mirrored by the Alexander and the classical path models. For the purposes of controlling the curvature of single microdomains, it is clear that the two models are essentially in agreement. As has been noted,[10] this is a consequence of the fact that the Alexander models overestimate the classical path free energies by a factor proportional to e^G so that the equilibrium free energy of the microphases are not at all well modeled, but the transitions between geometries are controlled by the ratio of stretching energies in the two blocks, so that the exponential overestimation does not affect phase boundaries much. It should be pointed out, however, that there is a systematic *quantitative* diference in the results, in that the phase boundary shifts in the Alexander model are more harsh than that predicted in the classical path model, a symptom of the exponential overestimation of free energies in the Alexander models. The packing of the domains is the essential feature shared by both models, and as packing seems to be the dominant effect, it is quite possible that these results could be changed drastically when the domains are made to adopt realistic three-dimensional packings. Adapting configurational tempering[23] and off-lattice SCF formalisms[24,25] to the present problem could well yield profitable interesting results. However, up to the constraints of the unit-spherical/cylindrical approximation, there is little difference in the qualitative predictions of the models. Given that the classical path calculations are doable semianalytically up to the numerical results given in Table 1, it seems that the

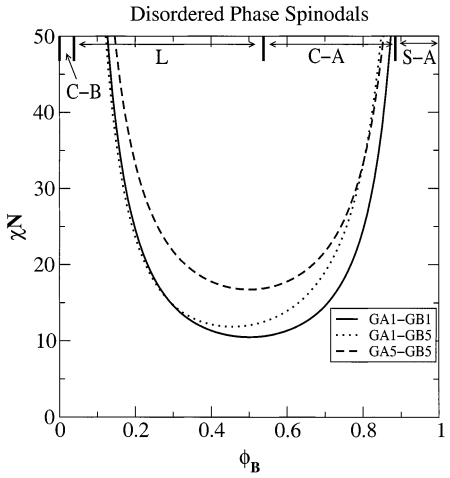

Figure 7. Disordered phase spinodal. Here the spinodals for G1G1 (solid line), GA1GB5 (dotted line), and G5G5 (dashed line) are shown. The G5G5 copolymer is more stable than the G1G1 copolymer toward creating a mesophase, but the difference between them narrows at large χN. The asymmetric copolymer interpolates between these two results. At the top of the figure are indicated the strong-segregation limit phase boundaries for the GA1GB5 copolymer.

classical path calculation has not only realism on its side but also, surprisingly, ease of computation.

5. Discussion

From Figures 5 and 6 it is clear that both the Alexander and SCF formulations predict sweeping changes to the diblock copolymer phase diagram and, further, that both theories predict roughly the same behavior. How well this predicted behavior matches the experimental behavior of such copolymer fluids depends on how well two assumptions are met, namely that the domains are in the strongly segregated regime and that the unit cell of the segregated pattern can be approximated as either spherical or circular in cross-section. Both of these issues will play a key role in determining the location and stability of the more exotic bicontinuous phases. Clearly, abandoning the circular/spherical unit cell is problematic in an analytic theory in the strong segregation limit, as the analysis of diblock copolymers along these lines is quite complex, involving partitioning the domains into wedge shapes for which nearly analytic results can be had.[21] A more direct approach is to employ an entirely numerical self-consistent field calculation either in real space on a highly symmetric lattice[10,22] or via a configurational tempering scheme[23] in the wavenumber space.[24,25] All three of these approaches are beyond the scope of the work contemplated here, however, and will be left to future studies.

The issue of "how strong" is strongly segregated can be addressed, however, without much further effort. While we assume here that γ and N are so large that strong segregation scaling is obtained, Figure 7 shows how well typical dendrimer−dendrimer copolymers might realize this limit. Plotted here is the disordered-phase spinodal as a function of χN as calculated in the second-order random phase approximation[26,27]

$$N\chi_{\text{spinodal}} = \min\left[\frac{NS(q)}{2W(q)}\right] \tag{60}$$

where $S(q)$ is the structure factor for an ideal AB dendrimer−dendrimer copolymer

$$S(q) = S_{AA}(q) + S_{BB}(q) + 2S_{AB}(q) \tag{61}$$

for radiation scattered with wavenumber $\vec{q}$. Here S_{AA} is the partial structure factor for just monomers of type A on an (ideal) chain, and S_{AB} is the A−B cross-correlation. Also

$$W(q) = \det[S_{ij}] = S_{AA}(q)S_{BB}(q) - S_{AB}{}^2(q) \tag{62}$$

The solid line in Figure 7 shows the location of the disordered phase spinodal for a G1G1 diblock, as originally calculated by Leibler.[27] The long-dashed line is the disordered phase spinodal for a G5G5 copolymer.[28] Making the copolymers be branched evidently stabilizes the disordered phase, so that achieving the strongly segregated regime might be expected to be correspondingly more difficult for these dendrimer−dendrimer copolymers. The enhancement in the compatibility of the block copolymer melt is only an approximately 50% increase in the lowest spinodal χN, while for very asymmetric mixtures, the spinodals are asymptotically equivalent. Interestingly, the spinodal for GA1GB5 diblocks, (dotted line) roughly mimics the linear diblock result at low ϕ_B and the $G_A = 5$ spinodal when ϕ_B is large. Thus, we can expect that dendrimer−dendrimer block copolymers will behave *less well segregated* than an equivalent linear diblock. Indeed, coupling the fact that symmetric $G_A = G_B$ copolymers all have the same asymptotic strong-segregation phase boundaries with the compatibilizing effect of increasing the degree of branching leads one to expect that the branching of the chains might be a worthwhile experimental avenue for studying the extreme-weak segregation limit of block copolymers. Whether or not this suppression of fluctuations with increasing branching can produce a true second-order transition at $\phi_B = 0.5$ is an intriguing question whose answer surely requires more analysis that has been carried out here. As a first step, the RPA perturbation scheme should be carried out on these dendrimer−dendrimer copolymers to determine the weak-segregation phases.

The fact that these dendrimers[28] display an internal nonideal structure depending on generation number and degree of polymerization puts a further limit on the molecular weight of the chains. Considering just the A block, which contains $n_A(2_A{}^G - 1)$ monomers, the typical ideal radius of gyration of this subchain scales as $R_g \approx \sqrt{n_A G_A}$, so that the internal density of a single ideal hyperbranched coil is

$$\rho = \frac{N_{\text{tot}}}{R_g{}^3} \tag{63}$$

which completely fills space when $\rho = 1$. In order for the chains to be nearly ideal for the computation of the spinodal based on Gaussian scattering functions

$$N \gg \left|\frac{2^{G_A} - 1}{G_A}\right|^3 \tag{64}$$

Thus, for $G_A = 5$, we require $N_{\text{tot}} \gg 240$, while for $G_A = 10$, it is necessary for $N_{\text{tot}} \gg 10^6$. Thus, for $G < 10$ and typical polymer χ's on the order of 0.01−0.1, segregation parameters between $\chi N_{\text{tot}} = 2$ and $\chi N_{\text{tot}} = 10^4$ cover the

ideal range. It should be possible to observe the strongly segregated G5G5 regime, while extremely small values of χ (perhaps induced by deuteration) will be necessary to observe the weakly segregated regime for G10G10 copolymers.

The full exploration of the weak-segregation limit behavior of these copolymers, and even the location of the mean-field critical point on the calculated spinodals, requires higher order contributions to the system free energy than is taken in the second-order RPA. One of the most interesting possibilities involves $G_A = G_B$ dendrimers, for which the spherical phases in the strong segregation limit are suppressed. Determining if these phases are suppressed for *all* χN would seem to be the most interesting pressing question. That analysis is straightforward, however, and will be the subject of future work.

It should be kept in mind that there are other, complementary, methods for shifting the phase boundaries in block copolymer melts. In the above, it was assumed that the polymers involved are conformationally symmetric, that is are composed of monomers with exactly the same size. While for simplicity's sake we have focused here only on the effect that branching can have, it will be most interesting to determine whether the phase-boundary shifts observed with unequal branching can be partially canceled by such a conformational asymmetry.[29] Such a treatment would be necessary for making quantitative predictions for specific hyperbranched copolymers. Going beyond the spherical unit cell approximation is likewise necessary for making precision predictions.[24,25] Relaxing the incompressibility assumption is a much more subtle enterprise and requires detailed knowledge of the equation of state of the ordered materials.[30]

6. Conclusion

The flexible-dendrimer copolymer phase diagram has been calculated in the classical path approximation, and compares favorably to a numerical calculation with an Alexander−de Gennes model. As previously predicted, the hyperbranching of one of the species is sufficient to dramatically swing the microphase diagram toward low values of branched volume fraction. All dendrimers satisfying $G_A = G_B$ have the same stongly segregated phase diagram, curiously without spherical phases, the result of chain-end exclusion zones being filled-in. As the dendrimers become more branched, it may be more difficult to achieve the strongly segregated regime.

Acknowledgment. The support of the Research Corporation (Grant CC5207) is gratefully acknowledged.

References and Notes

(1) Tomalia, D. A.; Baker, H.; Dewald, J.; Hall, M.; Martin, S.; Roeck, J.; Ryder, J.; Smith, P. *Polym. J.* **1985**, *17*, 117.
(2) Balogh, L.; Tomalia, D. A.; Hagnauer, G. L. *Chem. Innovation* **2000**, *30*, 19.
(3) Voegtle, F.; Gestermann, S.; Hesse, R.; Schwierz, H.; Windisch, B. *Prog. Polym. Sci.* **2000**, *25*, 987.
(4) Kimura, M.; Kato, M.; Muto, T.; Hanabusa, K.; Shirai, H. *Macromolecules* **2000**, *33*, 1117.
(5) Coen, M. C.; Lorenz, K.; Kressler, J.; Frey, H.; Muelhaupt, R.; *Macromolecules* **1996**, *29*, 8069.
(6) Irvine, D. J.; Mayes, A. M.; Satija, S. K.; Barker, J. G.; Sofia-Allgor, S. J.; Griffith, L. G. *J. Biomed. Mater. Resch.* **1998**, *40*, 498.
(7) Daoud, M.; Cotton, J. P. *J. Phys. (Paris)* **1982**, *43*, 531.
(8) Milner, S. T. *Macromolecules* **1994**, *27*, 2333.
(9) Frischknecht, A.; Fredrickson, G. H. *Macromolecules* **1999**, *32*, 6831.
(10) Pickett, G. T. *Macromolecules* **2002**, *35*, 1896.
(11) Aoi, K.; Motoda, A.; Ohno, M.; Tsutsumiuchi, K.; Okada, M.; Imae, T. *Polym. J.* **1999**, *31*, 1071.
(12) Alexander, S. *J. Phys. (Paris)* **1977**, *38*, 983.
(13) de Gennes, P.-G. *J. Phys. (Paris)* **1976**, *36*, 1443.
(14) de Gennes, P.-G.; Hervet, H. *J. Phys. (Paris)* **1983**, *44*, L351.
(15) Lescanec, R. L.; Muthukumar, M. *Macromolecules* **1990**, *23*, 2280.
(16) Semenov, A. N. *Sov. Phys. JTEP* **1985** *61* 733.
(17) Milner, S. T.; Witten, T. A.; Cates, M. E. *Macromolecules* **1988**, *21*, 2610.
(18) Pickett, G. T. *Macromolecules* **2001**, *34*, 8784.
(19) While this result holds in ref 10, it was not recognized in that work that the free-energy per chain was actually independent of z_o.
(20) Ball, R. C.; Marko, J. F.; Milner, S. T.; Witten, T. A. *Macromolecules* **1991**, *24*, 693.
(21) Olmsted, P. D.; Milner, Scott, T. *Macromolecules* **1998**, *31*, 4011.
(22) K. Huang, K.; Balazs, A. C. *Phys. Rev. Lett.* **1991**, *66*, 620.
(23) Drolet, F.; Fredrickson, G. H. *Phys. Rev. Lett.* **1999**, *83*, 4317.
(24) Matsen, M. W.; Schick, M. *Phys. Rev. Lett.* **1994**, *72*, 2660.
(25) Matsen, M. W.; Bates, F. S. *Macromolecules* **1996**, *29*, 1091.
(26) de Gennes, P.-G. *Scaling Concepts in Polymer Physics*; Cornell University Press: Ithaca, NY, 1979.
(27) Leibler, L. *Macromolecules* **1980**, *13*, 1602.
(28) Boris, D.; Rubinstein, M. *Macromolecules* **1996**, *29*, 7251.
(29) Matsen, M. W.; Bates, F. S. *J. Polym. Sci. B, Part B* **1997**, *35*, 945.
(30) Schweizer, K. S.; Curro, J. G. *Adv. Chem. Phys.* **1997**, *98*, 1; *Adv. Polym. Sci.* **1994**, *116*, 319.

MA021306O